RSC Advances

PAPER

View Article Online
View Journal | View Issue

Cite this: *RSC Adv.*, 2021, **11**, 15921

Preparation and dye adsorption properties of an oxygen-rich porous organic polymer†

Guang Yang, Huimin Gao, Qingyin Li and Shijie Ren *

Porous organic polymers (POPs), allowing fine synthetic control over their chemical structures, have shown great promise for addressing environmental issues. The high specific surface area and abundant porous structures of POPs can provide large storage space to adsorb dye molecules. Meanwhile, the introduction of polar groups, such as oxygen-containing functional groups in POPs, can not only improve the hydrophilicity, but also provide a strong interaction with dye molecules, thereby improving their adsorption performance. In this paper, an oxygen-rich porous polymer, POP-O, containing polar carbonyl and hydroxyl groups, was prepared by Sonogashira–Hagihara cross-coupling polycondensation. The characteristic results show that POP-O exhibits a hierarchical pore structure with a high specific surface area of 619 m^2 g^{-1}. The combination of abundant polar functional groups and high porosity endows POP-O with decent dye adsorption performance, and its theoretical maximum adsorption capacity for Rhodamine B (Rh B) is calculated to be 1012 mg g^{-1}.

Received 20th February 2021
Accepted 23rd April 2021

DOI: 10.1039/d1ra01382c

rsc.li/rsc-advances

Introduction

Organic dyes in wastewater from paper printing, textile dyeing, and plastic and food industries are one of the main sources of water pollution,[1,2] and they are highly hazardous to the aquatic environment and potentially damaging to human health. Adsorption is the most direct and effective way to remove contaminants from water.[3,4] Many porous materials with high specific surface area and rich porous structures such as activated carbons,[5,6] zeolites[7,8] and porous organic polymers (POPs),[9–11] have been used as adsorbents to remove organic dyes from wastewater. Among them, POPs are attracting more and more attention because of their unique advantages, such as structural diversity, adjustable porosity and ease of functionalization.

In order to achieve high adsorption capacity and selectivity for specific organic substances, tailor-designed functional moieties are often introduced into the porous polymer structures.[12–14] Generally, there are two methods to introduce special functional groups into the porous polymers and the first one is the post-functionalization method.[15] For example, Fang *et al.* synthesized polyarylether-based covalent organic frameworks (COFs) with carboxyl or amino groups being functionalized through post-modification process, achieving the removal of antibiotics from water over a wide pH range.[16] Song *et al.* prepared cationic conjugated microporous polymers (CMPs) by post-polymerization functionalization and found that the introduction of cations was beneficial to increasing the adsorption rate and amount of anionic dyes such as Congo red and methyl orange.[17] However, the degree of post-functionalization reaction is usually low and it may cause the damage of the polymer structure during the post-modification process. The other functionalization way is the bottom-up method,[18] which involves the direct polymerization of the functional group containing monomers. This method could accurately control the amounts and locations of functional groups without damaging the structure of POPs. Some special functional groups such as hydroxyl (–OH),[19] amino ($–NH_2$),[20] carboxyl (–COOH)[21] and sulfonic acid ($–SO_3H$) groups[22] have been introduced into POPs through the bottom-up method and the functionalized POPs have been extensively used in the field of dye adsorption.

Among these functional groups, oxygen-containing functional groups could bring about some special properties, when they are incorporated into POPs.[23,24] Firstly, the presence of oxygen-containing groups can increase hydrophilicity of the POPs and thus expand the contact area between POPs and the dye molecules in water. Also, the oxygen-rich units could make the functionalized POPs more electronegative, affording additional electrostatic interactions with cationic dye molecules.[25] Cooper *et al.* found that the introduction of hydrophilic hydroxyl groups can improve the dye adsorption capacity of CMPs.[19] Liu *et al.* prepared a novel triterpene and crown ether-based porous copolymer POP-TCE-15, and found that there was electrostatic interaction between the lone pair of electrons on the O atom of crown-ether-15 and the positively charged cationic dye methylene blue.[26] Although recent studies have

College of Polymer Science and Engineering, State Key Laboratory of Polymer Materials Engineering, Sichuan University, Chengdu, 610065, P. R. China. E-mail: rensj@scu.edu.cn

† Electronic supplementary information (ESI) available. See DOI: 10.1039/d1ra01382c

shown that introducing oxygen-containing groups could display significant effects on the adsorption performance of the POPs, the synergistic effect between different oxygen-containing functional groups still needs to be studied. Based on the above considerations, a novel oxygen-rich POP, containing polar carbonyl and hydroxyl groups, was synthesized *via* Sonogashira–Hagihara cross-coupling polycondensation. The effects of pore structure and polar groups on the adsorption performance were discussed. Density functional theoretical (DFT) calculation revealed that the carbonyl and hydroxyl groups of POP-O ensured high binding energy toward Rh B molecules.

Experimental

Materials

2,5-Dichloro-3,6-dihydroxy-*p*-benzoquinone was purchased from TCI, trimethylsilyl acetylene, 1,4-dibromobenzene, 1,3,5-tribromobenzene, tetrakis(triphenylphosphine)palladium ($Pd(PPh_3)_4$), copper(I) iodide (CuI), trimethylamine (TEA), and *N*,*N*-dimethylformamide (DMF) were all purchased from Adamas. 1,3,5-Triethynylbenzene was synthesized by previously reported literature methods.[27] The NMR spectrum of 1,3,5-triethynylbenzene is shown in Fig. S1.†

Synthesis of polymers

Experimentally, 1,3,5-triethynylbenzene (150 mg, 1 mmol), 2,5-dichloro-3,6-dihydroxy-*p*-benzoquinone (209 mg, 1 mmol), $Pd(PPh_3)_4$ (58 mg, 0.05 mmol) and CuI (19 mg, 0.1 mmol), were dissolved in the mixture of DMF (20.0 mL) and TEA (20.0 mL). The reaction mixture was heated to 80 °C and stirred for 72 h under argon atmosphere. Then deionized water was added into the resultant solution after it was cooled down to room temperature. The polymer collected by filtration was washed thoroughly with water, methanol, dichloromethane and acetone. Further purification of the polymer was achieved by Soxhlet extraction with methanol, chloroform and tetrahydrofuran. The product was dried in vacuum for 24 h at 80 °C and POP-O was obtained in 72% yield as a brown solid.

For comparison, a structural analogue polymer without oxygen-containing polar groups, POP-B, was synthesized (Scheme S1†) according to the literature.[19]

Characterization

Fourier transformed infrared (FT-IR) spectra were recorded in transmission mode on a Bruker VERTEX 70 FT-IR spectrometer. ^{13}C CP-MAS (cross-polarization magic-angle-spinning) solid-state NMR was recorded on BRUKER AVANCE III HD 400 MHz NMR spectrometer. Elemental analysis was measured by Elementer Vario EL elemental analyzer. The thermal stability of POP-O was evaluated by thermogravimetric analysis (TGA) under N_2 atmosphere with a heating rate of 5 °C min^{-1} and over the temperature range of 30–800 °C. X-ray diffraction (XRD) was carried out on Philips X' Pert Pro. Scanning electron microscopy (SEM) images of POP-O were obtained by the Nova Nano SEM 450 scanning electro-microscope. Transmission electron microscopy (TEM) images of the POP-O were performed on the Tecnai G2 F30 (FEI Holland) transmission electron microscope. Surface area and pore size distributions (PSDs) (77 K) were measured by using Belsorp-Max Automatic Micropore Adsorption Analyzer. Before analysis, the sample was degassed in a vacuum at 120 °C for 12 h. The surface area was calculated based on nitrogen adsorption isotherms by Brunauer–Emmett–Teller (BET). Ultraviolet-visible spectra were measured on a UV-vis-NIR spectrophotometer (UV-3600) at room temperature, over the wavelength range of 400–800 nm. The particle size distribution and zeta potential were measured by the Nano-ZS Malvern instrument.

Dye adsorption measurement

Experimental operation: at a temperature of 298 K, 10 mg of the polymer was weighed into multiple glass bottles containing 20 mL of Rh B solution at various concentrations, and the mixture was agitated at 180 rpm for different time intervals. After adsorption, the polymer is filtered and the absorbance of the remaining solution is measured by UV-vis spectra to obtain the resultant dye concentration (characteristic absorbance peak of Rh B is 554 nm).

The calculation formula of the adsorption capacity of the polymer to Rh B is:

$$q = \frac{(C_0 - C_t)\ V}{m}$$

Among them, C_0 is the initial concentration of Rh B aqueous solution (mg L^{-1}); C_t is the concentration of Rh B in the solution in t hour (mg L^{-1}); V is the volume of Rh B aqueous solution (L); m is the mass of polymer (g).

The Langmuir and Freundlich models were used to fit the adsorption isotherm. Rh B aqueous solutions with initial concentrations of 214, 276, 328, 481, 498, 546 and 663 mg L^{-1} were selected for testing, and the sampling time was 18 h.

The Langmuir equation is:

$$\frac{C_e}{q_e} = \frac{1}{K_L q_m} + \frac{C_e}{q_m}$$

The Freundlich equation is:

$$\ln q_e = \ln K_F + \frac{1}{n} \ln C_e$$

Among them, q_m is the maximum adsorption capacity of Rh B by polymer (mg g^{-1}); C_e is the equilibrium concentration (mg L^{-1}); K_L is the Langmuir constant; K_F is the Freundlich constant; and $1/n$ is the adsorption index.

A pseudo-first-order[28] kinetic model and pseudo-second-order kinetic model[29] were used to fit the kinetic process of polymer adsorption of Rh B.

The formula of the pseudo-first-order kinetic model is:

$$q_t = q_e(1 - e^{-kt})$$

The formula of the pseudo-first-order kinetic model is:

$$\frac{t}{q_t} = \frac{1}{k_2 q_e^2} + \frac{t}{q_e}$$

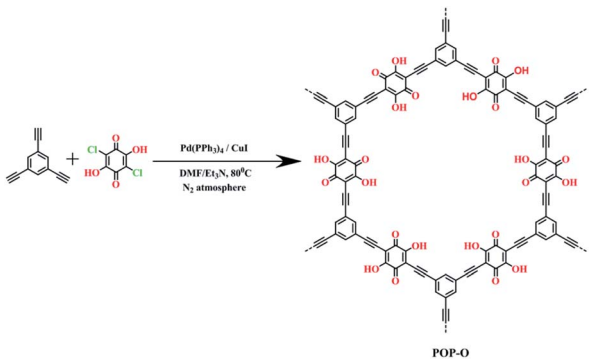

Scheme 1 Synthetic route of the polymer POP-O.

Among them, q_e is the equilibrium adsorption capacity of Rh B by polymer (mg g^{-1}); q_t is the adsorption capacity of Rh B by polymer in t hour (mg g^{-1}); k_1 is the pseudo-first-order fitting constant; k_2 is pseudo-second-order fitting constant; t is time (h).

Results and discussion

Synthesis and characterization

The POP-O was synthesized by Sonogashira–Hagihara cross-coupling polycondensation according to the procedure shown in Scheme 1. The monomer 1,3,5-triethynylbenzene with three functionalities is used as the strut to construct the network structure and the comonomer 2,5-dichloro-3,6-dihydroxy-*p*-benzoquinone containing polar carbonyl and hydroxyl groups, is chosen as the oxygen-rich moiety. Due to the crosslinked skeleton, the obtained POP-O was insoluble in common organic solvents such as dichloromethane, tetrahydrofuran, methanol, acetone, *N*,*N*-dimethylformamide. The chemical structure of POP-O is confirmed by Fourier transform infrared (FT-IR) spectroscopy and solid-state ^{13}C CP-MAS NMR. In the FT-IR spectra (Fig. S2†), the C–Cl absorption of POP-O at 1263 cm^{-1} almost disappear after the polycondensation, indicating high polymerization efficiency. FT-IR spectra also show characteristic absorbance bands at 1660 cm^{-1} and 3290 cm^{-1} corresponding to the C=O and O–H stretching vibrations, respectively, indicating the presence of carbonyl and hydroxyl groups. Moreover, solid state ^{13}C CP-MAS NMR spectra of POP-O (Fig. S3†) shows that aromatic carbon displays in broad peaks from 110 to 150 ppm and two characteristic broad peaks of ethynyl groups could be found at 80 to 90 ppm.[30] Meanwhile, the elemental analysis of the polymer shows that the mass fractions of carbon atoms and hydrogen atoms in POP-O are 68.86% and 2.1% respectively, which are basically consistent with the theoretical content, further confirming the chemical structure of the POP-O.

Thermogravimetric analysis curve (TGA) of POP-O is shown in Fig. S4.† The first weight loss (10.9%) stage of POP-O was around 210 °C, which could be assigned to the weight loss of the adsorbed solvent. The following weight loss of the polymer could be further attributed to the decomposition of the framework. Because there is a certain amount of hydroxyl groups in the polymer structure, compared with other POPs, the thermal stability of the POP-O is slightly inferior.[31–33] The powder X-ray diffraction pattern of POP-O shows a broad peak in the range of 5–35° without obvious sharp peaks (Fig. S5†), indicating the amorphous structure of POP-O. The morphology of polymer is investigated by scanning electron microscopy (SEM) and transmission electron microscopy (TEM). It could be observed that the POP-O manifests as irregular particle accumulation (Fig. 1a–c). As can be seen from the TEM images (Fig. 1d–f), POP-O exhibits as flake shape. These particles assembled from flakes can help improve the contact area between the polymer and the organic dye.[34] In order to understand the hydrophilic property of the material, the contact angle between POP-O and water is tested (Fig. S6†). POP-O shows a contact angle with water of 60°, while POP-B exhibits a contact angle with water of 109°, indicating that the oxygen-containing functional groups could improve the hydrophilic property of the polymer. Decent hydrophilicity makes POP-O easier to form a uniform dispersion in aqueous solution, thereby helping to improve the adsorption performance.

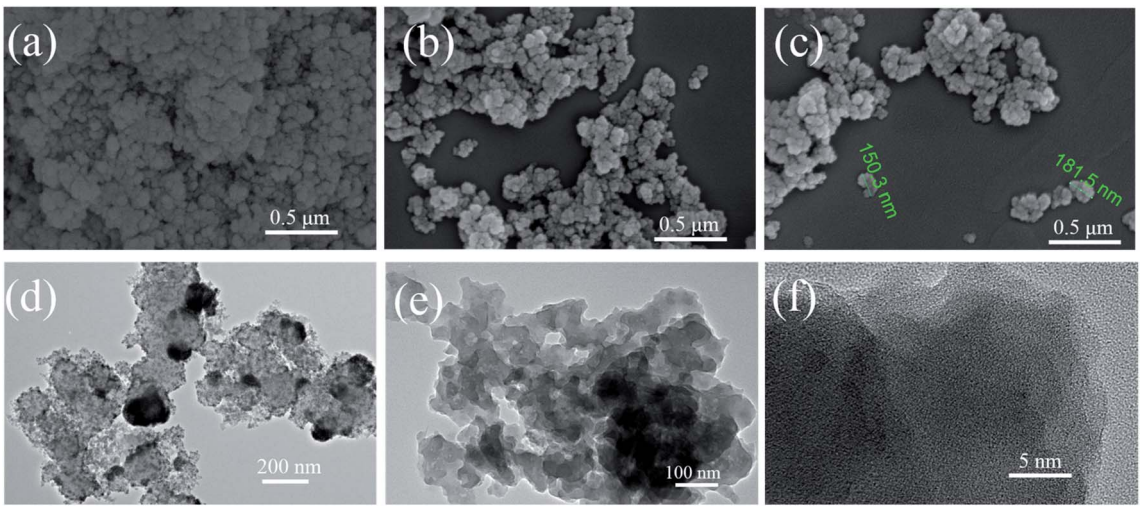

Fig. 1 (a–c) Scanning electron microscopy (SEM) images of POP-O; (d–f) transmission electron microscopy (TEM) images of POP-O.

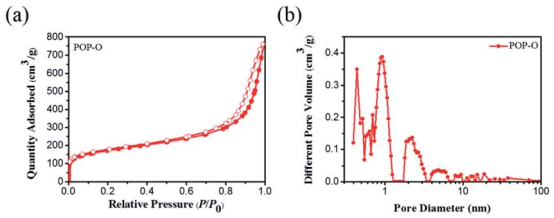

Fig. 2 Nitrogen adsorption–desorption isotherm (a) and pore size distribution (b) of the polymer POP-O.

Porosity of POP-O

The porosity of POP-O is measured by nitrogen adsorption and desorption experiments at 77 K. As shown in Fig. 2a, POP-O shows a combination of Type I and Type IV sorption isotherms with a hysteresis loop. The specific surface area of the POP-O is calculated to be 619 m^2 g^{-1} by the BET model. The pore size distribution of POP-O is shown in Fig. 2b, which is obtained from the nonlocalized density functional theory (NLDFT). POP-O mainly has micropores around 0.9 nm and mesopores around 2.2 nm, and there are also some mesopores at 5–40 nm. The results indicate that there is a hierarchical pore structure in the polymer. This hierarchical pore structure combines the advantages of micropores and mesopores, which could improve the mass transfer rate of the material and facilitate the entry of dye molecules into POP-O, thereby increasing its application potential in the field of adsorption.

Particle size and zeta potential

The adsorption performance of the polymer is not only related to its porosity, but also has an important relationship with the particle size in the solution.[35,36] 10 mg of the polymer was sonicated in 20 mL of aqueous solution for 5 minutes, and then its particle size was measured through light scattering method. As shown in Fig. S7,† the particles of POP-O have two size distributions of 1000–1700 nm and 100–180 nm, which is consistent with the observation result of the SEM images. The large-sized particles are formed from the aggregation of small-sized nanoparticles. Meanwhile, the particle size distribution of POP-B only shows one peak centered at 1414 nm. Smaller particle size of POP-O is beneficial for the adsorption of dye molecules. To further characterize the stability of the colloidal dispersions, zeta potential of the obtained polymers were measured. It is found that POP-O shows a zeta potential value of −27.4 mV, while the zeta potential value of POP-B is −12.7 mV, indicating higher stability of the POP-O dispersion.

Dye adsorption properties of POP-O

With large amounts of oxygen-rich groups and hierarchical pore structure, POP-O could potentially possess good adsorption capabilities for organic dye pollutants from water. We used Rhodamine B (Rh B) as the adsorbate to study the adsorption properties of POP-O for water-soluble pollutants. Fast kinetic adsorption capacity is one of the key factors for adsorbent, which directly determines the actual adsorption efficiency of the adsorbent. Adsorption of Rh B solution at 25 °C with an initial concentration of 481 mg L^{-1} is shown in Fig. 3a. The adsorption amounts of Rh B by POP-O increases rapidly within the first hour, and then gradually reaches equilibrium (Table S1†). The POP-O displayed an absorption of 590 mg g^{-1} at equilibrium, and the adsorption capacity of the comparative analogue polymer POP-B is 390 mg g^{-1} in equilibrium. The experimental data of the Rh B adsorption onto POP-O is fitted to the Langmuir and Freundlich adsorption isotherm models respectively (Fig. S8a, b and Tables S2, S3†). It can be seen that the adsorption of Rh B by POP-O is more in line with the Langmuir isotherm adsorption equation (R^2 = 0.99367) than Freundlich isotherm adsorption equation (R^2 = 0.98591), indicating that the Rh B adsorption onto POP-O is probably in a monomolecular-layer manner.[7] The maximum adsorption capacity of POP-O toward Rh B can thus be calculated through Langmuir equation to be 1012 mg g^{-1}, which is better than the adsorption capacity of many organic porous materials that have been reported so far, as shown in Table 1. The excellent adsorption capacity of POP-O for Rh B is mainly attributed to the following reasons. Firstly, due to the presence of hydroxyl and carbonyl groups, the POP-O has good hydrophilicity, which make POP-O easier to form a uniform dispersion in Rh B

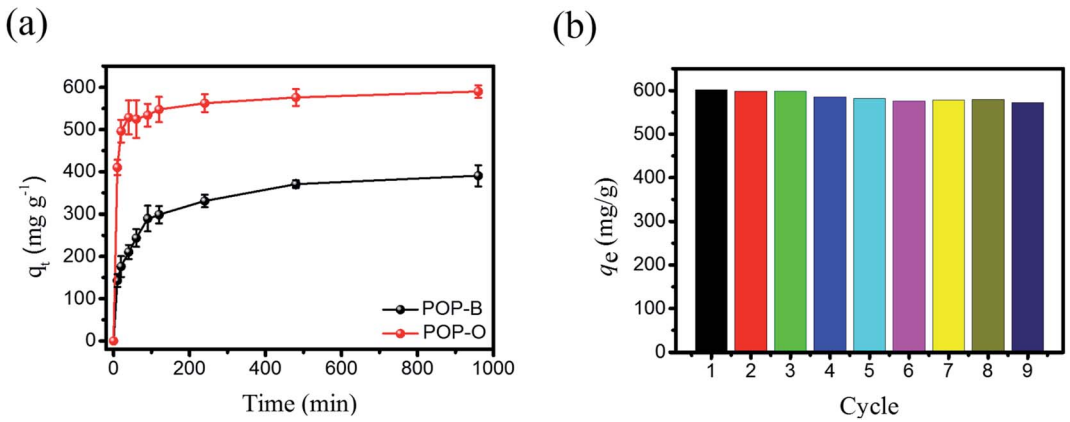

Fig. 3 (a) The adsorption capacity of Rh B by polymers over time; (b) recyclability of POP-O for the Rh B adsorption.

Table 1 Comparison of the maximum equilibrium adsorption capacity of different porous polymers towards Rh B at room temperature

Adsorbents	q_{max} (mg g^{-1}) of Rh B	Ref.
HJ-1	73.5	37
CoOF	72.15	38
SA-MMNPs	216	39
PDVB-VI	260.42	40
C-NSA_{Naph}HCP@Br	142	41
POP-TCE-15	421.9	26
CuP-DMNDA-COF/Fe	424	10
h-COP-P	460	42
DPT-HPP	256.40	43
CTF-CTTD	684.9	44
Noria-POP-1	855	45
HCPs-5%	1400	46
AzoPPOP	1357.58	47
POP-O	1012	This work

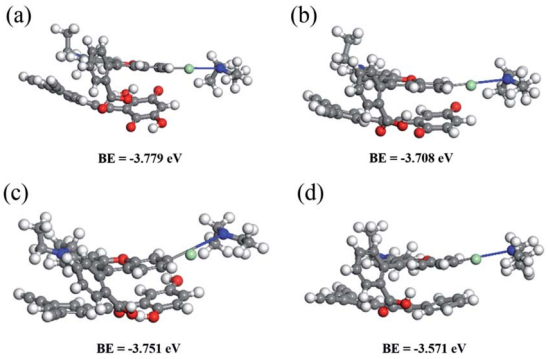

Fig. 4 Binding energies of Rh B molecule with the segments of polymers network (C, gray; N, blue; H, white; O, red; Cl, green) (a) the POP-O segment; (b) POP-O analogue with only carbonyl groups; (c) POP-O analogue with only hydroxyl groups; (d) POP-O analogue without carbonyl and hydroxyl groups.

aqueous solution. Secondly, the oxygen-rich units make POP-O electronegative, which allow additionally strong electrostatic interactions with cationic dye molecules (Rh B). The last but not least, the large specific surface area of POP-O provides a large storage space for the adsorption of dye molecules. The schematic adsorption process is shown in Fig. S9†. When POP-O is added to the aqueous solution of Rh B, the electronegative POP-O interacts with Rh B electrostatically. Meanwhile, the hierarchical pore structure is also beneficial to the adsorption of Rh B.

Pseudo-first-order and pseudo-second-order kinetic models are employed to fit the adsorption kinetic data (Fig. S10a, b and Table S4†), and the corresponding fitting parameters in Table S4† show that the pseudo-second-order kinetic model can better describe the kinetic data due to the higher correlation coefficient ($R^2 = 0.99983$). The results indicate that dye adsorption process appears to be controlled by the chemisorption process involving covalent forces through sharing or exchange of electrons between surface functional groups of POP-O and the positive charged of Rh B.

Stability and recycling are very important for POPs to be used as an adsorbent for industrial applications. The recyclability of POP-O for adsorption of Rh B was evaluated for nine cycles under the same condition. Before each run, the used POP-O was washed several times in ethanol until the colour of the filtrate became clear. The adsorption capacity of the POP-O in the nine adsorption cycles is shown in Fig. 3b. No loss of Rh B adsorption capacity is observed, indicating that POP-O has good adsorption stability and recyclability. Meanwhile, the SEM images, FT-IR spectra and PXRD patterns of POP-O were tested after the cycles, and found that there were no significant changes (Fig. S11–S13†).

To clarify the possible mechanism of the adsorption process, the binding energies (BEs, $BE = E_{total} - E_{segment} - E_{Rh\ B}$)[48] between the Rh B molecule and polymer segments are calculated by density functional theory (DFT) using Materials Studio software with the GGA-PBE basis set as shown in Fig. 4. The other three scaffolds only containing carbonyl or hydroxyl or neither were selected as model systems for comparison. After the optimization of all the moieties and their complexes, a difference in binding energies (BEs) is found where the POP-O segment shows the maximum BE toward Rh B with a value of −3.779 eV (Fig. 4). The results of the theoretical analysis show that the synergistic effect of different oxygen-containing functional groups in POP-O has a crucial influence on the Rh B adsorption ability. According to the experimental results and DFT calculations, it is suggested that the structural features of abundant oxygen-containing groups, high surface area, and hierarchical pore structures of POP-O work together to achieve excellent adsorption performance of Rh B dyes from aqueous solutions.

Conclusions

In summary, an oxygen-rich POP(POP-O) was prepared through Sonogashira–Hagihara cross-coupling polycondensation using monomers containing carbonyl and hydroxyl groups. The introduction of polar groups in POP-O not only improves the hydrophilicity, which makes POP-O easier to form a uniform dispersion in Rh B aqueous solution, but also can make POP-O more electronegative, which allows additionally strong electrostatic interactions with Rh B. Meanwhile, the high specific surface area of POP-O and the presence of hierarchical pore structure can provide a large storage space to adsorb dye molecules. POP-O exhibits excellent dye adsorption performance, and theoretical maximum adsorption capacity for Rh B can reach 1012 mg g^{-1}. This result indicates that through delicate structure design, functional POPs can be used as effective adsorbents for water treatment.

Conflicts of interest

There are no conflicts to declare.

Acknowledgements

This work is financially supported by National Natural Science Foundation of China (51973128) and Science and Technology Department of Sichuan Province (2019YJ0128).

References

1 A. Alsbaiee, B. J. Smith, L. Xiao, Y. Ling, D. E. Helbling and W. R. Dichtel, *Nature*, 2016, **529**, 190–194.
2 M. A. Shannon, P. W. Bohn, M. Elimelech, J. G. Georgiadis, B. J. Mariñas and A. M. Mayes, *Nature*, 2008, **452**, 301–310.
3 J. Zhang, Y. Wang, D. Liang, Z. Xiao, Y. Xie and J. Li, *Ind. Eng. Chem. Res.*, 2020, **59**, 14531–14536.
4 X. Xie, X. Huang, W. Lin, Y. Chen, X. Lang, Y. Wang, L. Gao, H. Zhu and J. Chen, *ACS Omega*, 2020, **5**, 13595–13600.
5 C. Patawat, K. Silakate, S. ChuanUdom, N. Supanchaiyamat, A. J. Hunt and Y. Ngernyen, *RSC Adv.*, 2020, **10**, 21082–21091.
6 S. Moosavi, C. W. Lai, S. Gan, G. Zamiri, O. Akbarzadeh Pivehzhani and M. R. Johan, *ACS Omega*, 2020, **5**, 20684–20697.
7 Y. Li, X. Yan, X. Hu, R. Feng and M. Zhou, *Chem. Eng. J.*, 2019, **375**, 122003.
8 W. Schwieger, A. G. Machoke, T. Weissenberger, A. Inayat, T. Selvam, M. Klumpp and A. Inayat, *Chem. Soc. Rev.*, 2016, **45**, 3353–3376.
9 Y. Yuan, H. Huang, L. Chen and Y. Chen, *Macromolecules*, 2017, **50**, 4993–5003.
10 Y. Hou, X. Zhang, C. Wang, D. Qi, Y. Gu, Z. Wang and J. Jiang, *New J. Chem.*, 2017, **41**, 6145–6151.
11 D. Shetty, I. Jahovic, J. Raya, F. Ravaux, M. Jouiad, J. C. Olsen and A. Trabolsi, *J. Mater. Chem. A*, 2017, **5**, 62–66.
12 J. Wang, G. Wang, W. Wang, Z. Zhang, Z. Liu and Z. Hao, *J. Mater. Chem. A*, 2014, **2**, 14028–14037.
13 F. T. Costa, K. V. Jardim, A. F. Palomec-Garfias, P. R. Caceres-Velez, J. A. Chaker, A. Medeiros, S. E. Moya and M. H. Sousa, *ACS Omega*, 2019, **4**, 5640–5649.
14 R. M. N. Kalla, M. R. Kim and I. Kim, *Ind. Eng. Chem. Res.*, 2018, **57**, 11583–11591.
15 W. Zhao, Y. Jiao, R. Gao, L. Wu, S. Cheng, Q. Zhuang, A. Xie and W. Dong, *Chem. Eng. J.*, 2020, **391**, 123591.
16 X. Guan, H. Li, Y. Ma, M. Xue, Q. Fang, Y. Yan, V. Valtchev and S. Qiu, *Nat. Chem.*, 2019, **11**, 587–594.
17 Y. Liu, Y. Cui, C. Zhang, J. Du, S. Wang, Y. Bai, Z. Liang and X. Song, *Chem.–Eur. J.*, 2018, **24**, 7480–7488.
18 N. Huang, L. Zhai, H. Xu and D. Jiang, *J. Am. Chem. Soc.*, 2017, **139**, 2428–2434.
19 R. Dawson, A. Laybourn, R. Clowes, Y. Z. Khimyak, D. J. Adams and A. I. Cooper, *Macromolecules*, 2009, **42**, 8809–8816.
20 P. Su, X. Zhang, Z. Xu, G. Zhang, C. Shen and Q. Meng, *New J. Chem.*, 2019, **43**, 17267–17274.
21 Y. Li, C. X. Yang, H. L. Qian, X. Zhao and X. P. Yan, *ACS Appl. Nano Mater.*, 2019, **2**, 7290–7298.
22 G. Xiong, B. B. Wang, L. X. You, B. Y. Ren, Y. K. He, F. Ding, I. Dragutan, V. Dragutan and Y. G. Sun, *J. Mater. Chem. A*, 2019, **7**, 393–404.
23 Y. Gan, G. Chen, Y. Sang, F. Zhou, R. Man and J. Huang, *Chem. Eng. J.*, 2019, **368**, 29–36.
24 K. Y. Yan, J. Y. Chen, X. Y. Li, Q. Wang and G. C. Kuang, *Macromol. Chem. Phys.*, 2020, **221**, 1900553.
25 R. Shen and H. Liu, *RSC Adv.*, 2016, **6**, 37731–37739.
26 T. Xu, Y. He, Y. Qin, C. Zhao, C. Peng, J. Hu and H. Liu, *RSC Adv.*, 2018, **8**, 4963–4968.
27 J. He, N. Wang, Z. Cui, H. Du, L. Fu, C. Huang, Z. Yang, X. Shen, Y. Yi, Z. Tu and Y. Li, *Nat. Commun.*, 2017, **8**, 1172.
28 J. Fu, Z. Chen, M. Wang, S. Liu, J. Zhang, J. Zhang, R. Han and Q. Xu, *Chem. Eng. J.*, 2015, **259**, 53–61.
29 T. Wang, K. Kailasam, P. Xiao, G. Chen, L. Chen, L. Wang, J. Li and J. Zhu, *Microporous Mesoporous Mater.*, 2014, **187**, 63–70.
30 X.-H. Zhang, X. P. Wang, J. Xiao, S. Y. Wang, D. K. Huang, X. Ding, Y.-G. Xiang and H. Chen, *J. Catal.*, 2017, **350**, 64–71.
31 H. Zhou, B. Zhao, C. Fu, Z. Wu, C. Wang, Y. Ding, B.-H. Han and A. Hu, *Macromolecules*, 2019, **52**, 3935–3941.
32 Y. Wang, H. Liu, Q. Pan, C. Wu, W. Hao, J. Xu, R. Chen, J. Liu, Z. Li and Y. Zhao, *J. Am. Chem. Soc.*, 2020, **142**, 5958–5963.
33 T. Xu, Y. Li, Z. Zhao, G. Xing and L. Chen, *Macromolecules*, 2019, **52**, 9786–9791.
34 Q. Huang, L. Guo, N. Wang, X. Zhu, S. Jin and B. Tan, *ACS Appl. Mater. Interfaces*, 2019, **11**, 15861–15868.
35 Y. Liu, C. y. Liu, L. b. Chen and Z. y. Zhang, *J. Colloid Interface Sci.*, 2003, **257**, 188–194.
36 S. Jang, J. Park, S. Shin, C. Yoon, B. K. Choi, M.-s. Gong and S.-W. Joo, *Langmuir*, 2004, **20**, 1922–1927.
37 J. H. Huang, K. L. Huang, S. Q. Liu, A. T. Wang and C. Yan, *Colloids Surf., A*, 2008, **330**, 55–61.
38 M. Barylak, K. Cendrowski and E. Mijowska, *Ind. Eng. Chem. Res.*, 2018, **57**, 4867–4879.
39 Q. Li, Z. Zhan, S. Jin and B. Tan, *Chem. Eng. J.*, 2017, **326**, 109–116.
40 Y. Han, W. Li, J. Zhang, H. Meng, Y. Xu and X. Zhang, *RSC Adv.*, 2015, **5**, 104915–104922.
41 X. Shen, S. Ma, H. Xia, Z. Shi, Y. Mu and X. Liu, *J. Mater. Chem. A*, 2018, **6**, 20653–20658.
42 H. J. Zhang, J. H. Wang, Y. H. Zhang and T. L. Hu, *J. Polym. Sci., Part A: Polym. Chem.*, 2017, **55**, 1329–1337.
43 M. G. Mohamed, A. F. M. El-Mahdy, T. S. Meng, M. M. Samy and S. W. Kuo, *Polymers*, 2020, **12**, 2426.
44 Q. Jiang, H. Huang, Y. Tang, Y. Zhang and C. Zhong, *Ind. Eng. Chem. Res.*, 2018, **57**, 15114–15121.
45 D. Jiang, R. Deng, G. Li, G. Zheng and H. Guo, *RSC Adv.*, 2020, **10**, 6185–6191.
46 S. Wang, L. Shao, Y. Sang and J. Huang, *J. Chem. Eng. Data*, 2019, **64**, 1662–1670.
47 Y. Chen, Y. Fang, J. Yu, W. Gao, H. Zhao and X. Zhang, *J. Hazard. Mater.*, 2021, **406**, 124769.
48 T. Xu, S. An, C. Peng, J. Hu and H. Liu, *Ind. Eng. Chem. Res.*, 2020, **59**, 8315–8322.